A coupled nonlinear continuum model for bifurcation behaviour of fluid-conveying nanotubes incorporating internal energy loss

Ali Farajpour [a*], Mergen H. Ghayesh [a], Hamed Farokhi [b]

[a] *School of Mechanical Engineering, University of Adelaide, South Australia 5005, Australia*

[b] *Department of Mechanical and Construction Engineering, Northumbria University, Newcastle upon Tyne NE1 8ST, UK*

[*] *Corresponding author's email: ali.farajpourouderji@adelaide.edu.au (A. Farajpour)*

Abstract

A coupled continuum model incorporating size influences and geometric nonlinearity is presented for the coupled motions of viscoelastic nonlinear nanotubes conveying nanofluid. A modified model of nanobeams incorporating nonlocal strain gradient effects is utilised for describing size influences on the bifurcation behaviour of the fluid-conveying nanotube. Furthermore, size influences on the nanofluid are taken into account via Beskok-Karniadakis theory. To model the geometric nonlinearity, nonlinear strain-displacement relations are employed. Utilising Hamilton's principle and the Kelvin-Voigt model, the coupled equations of nonlinear motions capturing the internal energy loss are derived. A Galerkin procedure with a high number of shape functions and a direct time-integration scheme are then employed to extract the bifurcation characteristics of the nanofluid-conveying nanotube with viscoelastic properties. A specific attention is paid to the chaotic response of the viscoelastic nanosystem. It is found that the coupled viscoelastic bifurcation behaviour is very sensitive to the flow velocity.

Keywords: Nanotubes; Nanofluid flow; Internal energy loss; Coupled motion; Nonlocal strain gradient model

1. Introduction

Fluid-conveying nanomechanical devices have a number of promising applications in nanotechnology involving drug delivery, cancer diagnosis and nanosensors. In fluid-conveying nanomechanical devices such as nanofluidic-based devices [1], the interactions between the fluid and the fundamental structure are of high significance since it affects the output/input response of the nanomechanical device.

Besides conducting experiments and molecular dynamics (MD) simulations, the application of continuum-based approaches to microscale and nanoscale structures has also been reported as these approaches pave the way for better understanding of experimental results [2-5]. Since the classical continuum-based approach does not have a scale parameter associated with molecular interactions, it should not be utilised for structures at small-scales [6-9]. To capture the influence of molecular interactions, the classical continuum mechanics has been modified in different ways [10-12], leading to a number of size-dependent theories such as the pure nonlocal elasticity (PNE) [13-17], couple stress models [18-22] and nonlocal strain gradient theory (NSGT) [23-27]. Employing MD calculations, it has recently been shown that the NSGT is reasonable for nanostructures [28]. In the present analysis, this modified continuum-based approach is employed for incorporating scale effects related to molecular interactions.

A considerable effort has been made to model the mechanics of nanotubes with small-scale effects. For instance, Sudak [29] explored the instability of nanotubes with small-scale effects via the nonlocal theory. In another paper, Murmu and Pradhan [30] examined thermo-mechanical oscillation of nanotubes resting on an elastic foundation. In addition, the mechanics of a system of carbon nanotubes and microtubules [31] as well as a system of

nanobeams and piezoelectric nanowires [32] were analysed using size-dependent beam models. Setoodeh et al. [33] provided an exact solution for the nonlinear buckling of nanotubes with small-scale effects; they applied the nonlocal theory of beams to capture small-scale effects. More recently, in addition to the nonlocal theory, the NSGT has been utilised for modelling nanotubes with small-scale effects [25, 34-36]. For example, Li and Hu [37] applied the NSGT so as to study wave dispersion in fluid-conveying nanotubes. Moreover, the large-amplitude dynamics of perfect nanotubes [38] and imperfect ones with geometrical imperfections [39] was studied applying the NSGT. Furthermore, Zhu and Li [40] employed an integral form of the NSGT to study the longitudinal dynamics of nanotubes.

The energy loss associated with internal frictions can considerably affect the mechanics of fundamental structures at nanoscales. To have a better prediction of the mechanical behaviours, it is advised to capture the effects of this phenomenon in continuum-based formulations. In this study, the effects of internal frictions are taken into consideration via employing the Kelvin-Voigt model.

The mechanical behaviours of fundamental nanoscale structures conveying fluid have been analysed in recent years via modified continuum-based approaches. An analytical model, for instance, was developed by Wang [41] to describe size influences on the vibration of fluid-conveying tubes at microscales. Employing the PNE, Lee and Chang [42] examined the size-dependent linear transverse vibrations of a carbon nanotube (CNT) containing nanofluid flow. The influences of a viscoelastic surrounding medium on the size-dependent mechanics of fluid-conveying CNTs were also studied by Soltani et al. [43]. In addition, the effects of couple stresses on the linear vibrations of fluid-conveying CNTs were examined by Zeighampour and Beni [44] via application of a modified continuum-based

approach. Zhen et al. [45] also studied the influences of a temperature rise on the size-dependent mechanics of CNTs containing nanofluid flow using a PNE-based approach. In another article, Khodami Maraghi et al. [46] developed a beam model incorporating size influences to explore the mechanical behaviours of boron nitride nanotubes conveying nanofluid. A PNE-based model was proposed by Liang and Su [47] for predicting the instability features of CNTs conveying pulsatile fluid. The influences of a nonlinear foundation together with thermal effects on the oscillations of fluid-conveying CNTs were also investigated by Askari and Esmailzadeh [48]. In another study, Ghasemi et al. [49] utilised the Euler-Bernoulli theory of nonlocal nanobeams for predicting size influences on the post-buckling of multi-walled CNTs conveying fluid at nanoscales. Moreover, Oveissi et al. [50] presented a PNE-based scale-dependent model to analyse the longitudinal vibrations and instability of fluid-conveying CNTs. In another paper, Bahaadini and Hosseini [17] have recently explored the influence of a magnetic field on the flutter instability of fluid-conveying nanoscale tubes. A NSGT-based linear model has also been proposed in the literature for analysing wave propagations in fluid-conveying CNTs [37].

The above-described valuable papers are limited to either linear continuum-based models or nonlinear elastic models incorporating only transverse deflections. To the best of our knowledge, the coupled chaotic motions of viscoelastic nonlinear nanotubes conveying fluid incorporating both axial and transverse displacements have not been explored yet. This motivates us to develop a size-dependent fluid-structure interaction model for examining this problem. A NSGT-based model of nanobeams is utilised for describing the influence of being at nanoscales on the mechanics of the tube. In addition, the size influence on the fluid is incorporated via Beskok-Karniadakis theory. The geometric nonlinearity is modelled through nonlinear strain components. The coupled equations of nonlinear motions

incorporating the internal energy loss are presented utilising Hamilton's principle together with the Kelvin-Voigt model. The bifurcation characteristics of the fluid-conveying nanosystem with viscoelastic properties are numerically calculated by a Galerkin's procedure with a high number of shape functions and a direct time-integration scheme. In addition to the bifurcation response, the time history, phase-plane plot and fast Fourier transform for both motion types are discussed and analysed.

2. Modified continuum-based modelling

A nanofluid-conveying nanotube with outer diameter d_o and length L is shown in Fig. 1. The nanoscale tube is assumed to be subject to an external excitation as depicted in the figure. A nanofluid flow with a constant velocity U is conveyed by the nanoscale tube. Large deflections are incorporated through the strain-displacement relation [51-53]. Indicating the longitudinal displacement of the tube mid-plane by u and the transverse one by w, the nonlinear longitudinal strain (ε_{xx}) is given by

$$\varepsilon_{xx} = \frac{\partial u}{\partial x} - z\frac{\partial^2 w}{\partial x^2} + \frac{1}{2}\left(\frac{\partial w}{\partial x}\right)^2. \tag{1}$$

In the present formulation, the stress resultants associated with the total NSGT stress $(\sigma^{(t)}_{xx(t)})$ are defined by

$$N_{xx(t)} = \int_A \sigma^{(t)}_{xx(t)} dA, \;\; M_{xx(t)} = \int_A z\sigma^{(t)}_{xx(t)} dA, \tag{2}$$

where A is the cross-sectional area. The total NSGT stress is expressed as [54]

$$\left[1-\left(e_0\ell_n\right)^2\nabla^2\right]\sigma_{xx(t)}^{(t)}=E\left(1-\ell_g^2\nabla^2\right)\left[\frac{\partial u}{\partial x}+\frac{1}{2}\left(\frac{\partial w}{\partial x}\right)^2\right]-zE\left(1-\ell_g^2\nabla^2\right)\frac{\partial^2 w}{\partial x^2}$$
$$+\eta\left(1-\ell_g^2\nabla^2\right)\left(\frac{\partial^2 u}{\partial t\partial x}+\frac{\partial w}{\partial x}\frac{\partial^2 w}{\partial t\partial x}\right)-z\eta\left(1-\ell_g^2\nabla^2\right)\frac{\partial^3 w}{\partial t\partial x^2}, \quad (3)$$

in which e_0, ℓ_n, ∇^2, E, ℓ_g and η are the calibration constant, internal characteristics length, Laplace operator, elasticity modulus, strain gradient parameter and viscosity constant, respectively [55]. The above constitutive equation includes two different size parameters: 1) nonlocal parameter ($e_0\ell_n$), and 2) strain gradient parameter (ℓ_g). In fact, the nonlocal parameter is associated with the size effect induced by the stress nonlocality at nanoscales while the strain gradient parameter accounts for the size effect due to the large gradient of deformations at nanoscales. These size parameters are generally obtained via experiments or molecular dynamics [56, 57]. Using Eqs. (1)-(3), one can obtain

$$\left[1-\left(e_0\ell_n\right)^2\nabla^2\right]N_{xx(t)}=EA\left(1-\ell_g^2\nabla^2\right)\left[\frac{\partial u}{\partial x}+\frac{1}{2}\left(\frac{\partial w}{\partial x}\right)^2\right]$$
$$+\eta A\left(1-\ell_g^2\nabla^2\right)\left(\frac{\partial^2 u}{\partial t\partial x}+\frac{\partial w}{\partial x}\frac{\partial^2 w}{\partial t\partial x}\right), \quad (4)$$

$$\left[1-\left(e_0\ell_n\right)^2\nabla^2\right]M_{xx(t)}=-EI\left(1-\ell_g^2\nabla^2\right)\frac{\partial^2 w}{\partial x^2}-\eta I\left(1-\ell_g^2\nabla^2\right)\frac{\partial^3 w}{\partial t\partial x^2}, \quad (5)$$

where *I* denotes the inertia moment. In the present formulation, the effects of strain gradients along *z* axis are not considered for simplification. Scale effects are usually assumed to be negligible along the thickness direction of nanobeams and nanoplates. Lately, NSGT-based beam models taking into consideration the thickness effect have been reported for the scale-dependent mechanical analysis of nanobeams [58-60]. The elastic energy variation (δU_e) and the viscous work variation (δW_v) can be written as

$$\delta U_e = \int_0^L \int_A \left(\sigma_{xx(e)} \delta \varepsilon_{xx} + \sigma^{(1)}_{xx(e)} \nabla \delta \varepsilon_{xx} \right) dA dx, \tag{6}$$

$$\delta W_v = -\int_0^L \int_A \left(\sigma_{xx(v)} \delta \varepsilon_{xx} + \sigma^{(1)}_{xx(v)} \nabla \delta \varepsilon_{xx} \right) dA dx. \tag{7}$$

Here $\sigma_{xx(e)}$ and $\sigma^{(1)}_{xx(e)}$, respectively, indicate the elastic zeroth-order and first-order nonlocal stresses while $\sigma_{xx(v)}$ and $\sigma^{(1)}_{xx(v)}$ denote the viscoelastic zeroth-order and first-order nonlocal stresses, respectively; moreover, ∇ is the gradient operator. Shear deformation effects are not considered in the formulation since in the present work, it is assumed that the thickness to length ratio of the nanotube is very small. Furthermore, based on the NSGT, it is assumed that the total stress is related to not only the zeroth-order nonlocal stress but also the first-order nonlocal stress. In fact, a higher-order stress is used in the NSGT in addition to the classical nonlocal stress. Taking into account this higher-order stress leads to a more comprehensive size-dependent model for nanotubes. The relations between different types of nonlocal stresses are given by [54]

$$\begin{aligned} \sigma^{(t)}_{xx(t)} &= \sigma_{xx(t)} - \nabla \sigma^{(1)}_{xx(t)}, \\ \sigma^{(t)}_{xx(e)} &= \sigma_{xx(e)} - \nabla \sigma^{(1)}_{xx(e)}, \\ \sigma^{(t)}_{xx(v)} &= \sigma_{xx(v)} - \nabla \sigma^{(1)}_{xx(v)}, \end{aligned} \tag{8}$$

and

$$\begin{aligned} \sigma^{(t)}_{xx(t)} &= \sigma^{(t)}_{xx(e)} + \sigma^{(t)}_{xx(v)}, \\ \sigma_{xx(t)} &= \sigma_{xx(e)} + \sigma_{xx(v)}, \\ \sigma^{(1)}_{xx(t)} &= \sigma^{(1)}_{xx(e)} + \sigma^{(1)}_{xx(v)}. \end{aligned} \tag{9}$$

In Eqs. (8) and (9), '*e*', '*v*' and '*t*' stand for the elastic, viscoelastic and total stresses, respectively. Indicating the mass per length of the nanotube by *m* and that of the nanofluid by *M*, the kinetic energy variation (δT_k) of the whole nanoscale system is expressed as

$$\delta T_k = m\int_0^L \left(\frac{\partial u}{\partial t}\frac{\partial \delta u}{\partial t} + \frac{\partial w}{\partial t}\frac{\partial \delta w}{\partial t} \right) dx$$
$$+M\int_0^L \left(\frac{\partial u}{\partial t} + \kappa_{BK}U + \kappa_{BK}U\frac{\partial u}{\partial x} \right)\left(\frac{\partial \delta u}{\partial t} + \kappa_{BK}U\frac{\partial \delta u}{\partial x} \right) dx \tag{10}$$
$$+M\int_0^L \left(\frac{\partial w}{\partial t} + \kappa_{BK}U\frac{\partial w}{\partial x} \right)\left(\frac{\partial \delta w}{\partial t} + \kappa_{BK}U\frac{\partial \delta w}{\partial x} \right) dx,$$

where

$$\kappa_{BK} = \left(\lambda Kn + 1\right)\left[\frac{4Kn}{\left(1-\beta Kn\right)}\left(\frac{2}{\sigma_v} - 1 \right) + 1 \right], \tag{11}$$

and

$$\lambda = \frac{2A}{\pi}\tan^{-1}\left[B\left(Kn\right)^C \right], \tag{12}$$

in which κ_{BK} is a correction factor incorporating the size influence on the nanofluid [61]; *Kn* indicates the Knudsen number. It should be noticed that Eqs. (11) and (12) are obtained using the Beskok-Karniadakis theory and assuming slip boundary conditions. The constant coefficients in the above relations are given as $\beta = -1$, $\sigma_v = 0.7$, $A = 64/\left(15\pi\right)$, $B = 4$ and $C = 0.4$. The external work related to the distributed loading ($\boldsymbol{q}_{ext}$) is formulated as

$$\delta W_q = \int_0^L q_{ext}\delta w \, \mathrm{d}x, \tag{13}$$

where

$$q_{ext} = \cos\left(\omega t\right)F\left(x\right). \tag{14}$$

Here ω and *F*(*x*) stand for the excitation frequency and loading amplitude, respectively. Substituting Eqs. (6), (7), (10) and (13) into the following principle

$$\int_{t_1}^{t_2}\left(\delta T_k + \delta W_q - \delta U_e + \delta W_v\right)\mathrm{d}t = 0, \tag{15}$$

one derives two motion equations as follows

$$\frac{\partial N_{xx(t)}}{\partial x} = \left(m+M\right)\frac{\partial^2 u}{\partial t^2} + 2M\kappa_{BK}U\frac{\partial^2 u}{\partial x \partial t} + M\kappa_{BK}^2U^2\frac{\partial^2 u}{\partial x^2}, \tag{16}$$

$$\frac{\partial^2 M_{xx(t)}}{\partial x^2}+\frac{\partial}{\partial x}\left(N_{xx(t)}\frac{\partial w}{\partial x}\right)+\cos(\omega t)F(x)=$$
$$(m+M)\frac{\partial^2 w}{\partial t^2}+2M\kappa_{BK}U\frac{\partial^2 w}{\partial x\partial t}+M\kappa_{BK}^2U^2\frac{\partial^2 w}{\partial x^2}. \tag{17}$$

Substituting Eqs. (4) and (5) into Eqs. (16) and (17), the coupled nonlinear equations in terms of axial and transverse displacements are derived as

$$\begin{aligned}
&(m+M)\frac{\partial^2 u}{\partial t^2}+2M\kappa_{BK}U\frac{\partial^2 u}{\partial t\partial x}+M\kappa_{BK}^2U^2\frac{\partial^2 u}{\partial x^2}\\
&-(e_0\ell_n)^2\nabla^2\left[(m+M)\frac{\partial^2 u}{\partial t^2}+2M\kappa_{BK}U\frac{\partial^2 u}{\partial t\partial x}+M\kappa_{BK}^2U^2\frac{\partial^2 u}{\partial x^2}\right]\\
&-EA\left(\frac{\partial^2 u}{\partial x^2}+\frac{\partial^2 w}{\partial x^2}\frac{\partial w}{\partial x}\right)+EA\ell_g^2\nabla^2\left(\frac{\partial^2 u}{\partial x^2}+\frac{\partial^2 w}{\partial x^2}\frac{\partial w}{\partial x}\right)\\
&-\eta A\left(\frac{\partial^3 u}{\partial t\partial x^2}+\frac{\partial w}{\partial x}\frac{\partial^3 w}{\partial t\partial x^2}+\frac{\partial^2 w}{\partial t\partial x}\frac{\partial^2 w}{\partial x^2}\right)\\
&+\eta A\ell_g^2\nabla^2\left(\frac{\partial^3 u}{\partial t\partial x^2}+\frac{\partial w}{\partial x}\frac{\partial^3 w}{\partial t\partial x^2}+\frac{\partial^2 w}{\partial t\partial x}\frac{\partial^2 w}{\partial x^2}\right)=0,
\end{aligned} \tag{18}$$

$$
\begin{aligned}
&-EI\frac{\partial^4 w}{\partial x^4}+EI\ell_g^2\nabla^2\frac{\partial^4 w}{\partial x^4}-\eta I\frac{\partial^5 w}{\partial t\partial x^4}+\eta I\ell_g^2\nabla^2\frac{\partial^5 w}{\partial x^4\partial t}\\
&+\cos(\omega t)F(x)-(e_0\ell_n)^2\nabla^2\cos(\omega t)F(x)\\
&+\left(1-(e_0\ell_n)^2\nabla^2\right)\left\{EA\frac{\partial^2 w}{\partial x^2}\left(1-\ell_g^2\nabla^2\right)\left[\frac{\partial u}{\partial x}+\frac{1}{2}\left(\frac{\partial w}{\partial x}\right)^2\right]\right.\\
&+EA\frac{\partial w}{\partial x}\left(1-\ell_g^2\nabla^2\right)\left(\frac{\partial^2 u}{\partial x^2}+\frac{\partial w}{\partial x}\frac{\partial^2 w}{\partial x^2}\right)\\
&+\eta A\frac{\partial^2 w}{\partial x^2}\left(1-\ell_g^2\nabla^2\right)\left(\frac{\partial^2 u}{\partial x\partial t}+\frac{\partial w}{\partial x}\frac{\partial^2 w}{\partial x\partial t}\right)\\
&+\eta A\frac{\partial w}{\partial x}\left(1-\ell_g^2\nabla^2\right)\left(\frac{\partial^3 u}{\partial x^2\partial t}+\frac{\partial^2 w}{\partial x\partial t}\frac{\partial^2 w}{\partial x^2}+\frac{\partial^3 w}{\partial x^2\partial t}\frac{\partial w}{\partial x}\right)\\
&+(e_0\ell_n)^2\frac{\partial^2 w}{\partial x^2}\left[(m+M)\frac{\partial^3 u}{\partial x\partial t^2}+2M\kappa_{BK}U\frac{\partial^3 u}{\partial x^2\partial t}+M\kappa_{BK}^2U^2\frac{\partial^3 u}{\partial x^3}\right]\\
&\left.+(e_0\ell_n)^2\frac{\partial w}{\partial x}\left[(m+M)\frac{\partial^4 u}{\partial x^2\partial t^2}+2M\kappa_{BK}U\frac{\partial^4 u}{\partial x^3\partial t}+M\kappa_{BK}^2U^2\frac{\partial^4 u}{\partial x^4}\right]\right\}\\
&=(m+M)\frac{\partial^2 w}{\partial t^2}+2M\kappa_{BK}U\frac{\partial^2 w}{\partial x\partial t}+M\kappa_{BK}^2U^2\frac{\partial^2 w}{\partial x^2}\\
&-(e_0\ell_n)^2\nabla^2\left[(m+M)\frac{\partial^2 w}{\partial t^2}+2M\kappa_{BK}U\frac{\partial^2 w}{\partial x\partial t}+M\kappa_{BK}^2U^2\frac{\partial^2 w}{\partial x^2}\right].
\end{aligned}
\tag{19}
$$

in which F_1 denotes a constant loading amplitude (i.e. $F(x)=F_1$).

3. Numerical solution

In this section, a numerical solution approach is developed via employing the Galerkin and direct time-integration methods. For convenience, first of all, a set of non-dimensional parameters is used as follows

$$
\begin{aligned}
&x^* = \frac{x}{L},\ u^* = \frac{u}{d_o},\ w^* = \frac{w}{d_o},\ r_A = \frac{AL^2}{I},\ s = \frac{L}{d_o},\\
&\chi_n = \frac{e_0 \ell_n}{L},\ \chi_g = \frac{\ell_g}{L},\ \eta^* = \frac{\eta}{E}\sqrt{\frac{EI}{L^4(m+M)}},\\
&\bar{M} = \frac{M}{M+m},\ t^* = t\sqrt{\frac{EI}{L^4(m+M)}},\ F^* = \frac{FL^4}{d_o EI},\\
&\omega^* = \omega\sqrt{\frac{L^4(m+M)}{EI}},\ U^* = U\sqrt{\frac{ML^2}{EI}},\ \bar{\nabla}^2 = \frac{\partial^2}{\partial x^{*2}}.
\end{aligned}
\tag{20}
$$

Using Eq. (20), the coupled motion equations given by Eqs. (18) and (19) can be rewritten in a non-dimensional form. According to the Galerkin scheme of decomposition, one can express the displacement components as

$$u(x,t) = \sum_{j=1}^{N_x} r_j(t)\Psi_j(x), \tag{21}$$

$$w(x,t) = \sum_{j=1}^{N_z} q_j(t)\Phi_j(x), \tag{22}$$

where r_j and q_j, respectively, indicate the longitudinal and transverse generalised coordinates whereas Ψ_j and Φ_j are the longitudinal and transverse shape functions, respectively. Employing the non-dimensional motion equations as well as Eqs. (21) and (22), one obtains

$$\frac{s}{r_A}\left[\sum_{j=1}^{N_x}\frac{d^2r_j}{dt^2}\left(\int_0^1\Psi_k\Psi_j dx\right)+2\kappa_{BK}\sqrt{\bar{M}}U\sum_{j=1}^{N_x}\frac{dr_j}{dt}\left(\int_0^1\Psi_k\frac{d\Psi_j}{dx}dx\right)\right.$$
$$\left.+\kappa_{BK}^2U^2\sum_{j=1}^{N_x}r_j\left(\int_0^1\Psi_k\frac{d^2\Psi_j}{dx^2}dx\right)\right]-\frac{s\chi_n^2}{r_A}\left[\sum_{j=1}^{N_x}\frac{d^2r_j}{dt^2}\left(\Psi_k\int_0^1\frac{d^2\Psi_j}{dx^2}dx\right)\right.$$
$$\left.+2\kappa_{BK}\sqrt{\bar{M}}U\sum_{j=1}^{N_x}\frac{dr_j}{dt}\left(\int_0^1\Psi_k\frac{d^3\Psi_j}{dx^3}dx\right)+\kappa_{BK}^2U^2\sum_{j=1}^{N_x}r_j\left(\int_0^1\Psi_k\frac{d^4\Psi_j}{dx^4}dx\right)\right]$$
$$-\int_0^1\Psi_k\frac{d}{dx}\left[s\sum_{j=1}^{N_x}r_j\frac{d\Psi_j}{dx}+\frac{1}{2}\left(\sum_{j=1}^{N_z}q_j\frac{d\Phi_j}{dx}\right)^2\right]dx$$
$$+\chi_g^2\int_0^1\Psi_k\frac{d^3}{dx^3}\left[s\sum_{j=1}^{N_x}r_j\frac{d\Psi_j}{dx}+\frac{1}{2}\left(\sum_{j=1}^{N_z}q_j\frac{d\Phi_j}{dx}\right)^2\right]dx$$
$$-\eta\int_0^1\Psi_k\frac{d}{dx}\left(s\sum_{j=1}^{N_x}\frac{dr_j}{dt}\frac{d\Psi_j}{dx}+\sum_{i=1}^{N_z}\sum_{j=1}^{N_z}q_i\frac{dq_j}{dt}\frac{d\Phi_i}{dx}\frac{d\Phi_j}{dx}\right)dx$$
$$+\eta\chi_g^2\int_0^1\Psi_k\frac{d^3}{dx^3}\left(s\sum_{j=1}^{N_x}\frac{dr_j}{dt}\frac{d\Psi_j}{dx}+\sum_{i=1}^{N_z}\sum_{j=1}^{N_z}q_i\frac{dq_j}{dt}\frac{d\Phi_i}{dx}\frac{d\Phi_j}{dx}\right)dx=0, \qquad (23)$$

$$\sum_{j=1}^{N_z}\frac{d^2q_j}{dt^2}\left(\int_0^1\Phi_k\Phi_j dx\right)+2\kappa_{BK}\sqrt{\bar{M}}U\sum_{j=1}^{N_z}\frac{dq_j}{dt}\left(\int_0^1\Phi_k\frac{d\Phi_j}{dx}dx\right)$$
$$+\kappa_{BK}^2U^2\sum_{j=1}^{N_z}q_j\left(\int_0^1\Phi_k\frac{d^2\Phi_j}{dx^2}dx\right)-\chi_n^2\left[\sum_{j=1}^{N_z}\frac{d^2q_j}{dt^2}\left(\int_0^1\Phi_k\frac{d^2\Phi_j}{dx^2}dx\right)\right.$$
$$\left.+2\kappa_{BK}\sqrt{\bar{M}}U\sum_{j=1}^{N_z}\frac{dq_j}{dt}\left(\int_0^1\Phi_k\frac{d^3\Phi_j}{dx^3}dx\right)+\kappa_{BK}^2U^2\sum_{j=1}^{N_z}q_j\left(\int_0^1\Phi_k\frac{d^4\Phi_j}{dx^4}dx\right)\right]$$
$$+\sum_{j=1}^{N_z}q_j\left(\int_0^1\Phi_k\frac{d^4\Phi_j}{dx^4}dx\right)-\chi_g^2\sum_{j=1}^{N_z}q_j\left(\int_0^1\Phi_k\frac{d^6\Phi_j}{dx^6}dx\right)$$
$$+\eta\sum_{j=1}^{N_z}\frac{dq_j}{dt}\left(\int_0^1\Phi_k\frac{d^4\Phi_j}{dx^4}dx\right)-\eta\chi_g^2\sum_{j=1}^{N_z}\frac{dq_j}{dt}\left(\int_0^1\Phi_k\frac{d^6\Phi_j}{dx^6}dx\right)-\left(\int_0^1\Phi_k dx\right)F_1\cos(\omega t)$$

$$
\begin{aligned}
&-\frac{r_A}{s^2}\int_0^1\Bigg\{\Phi_k\frac{d}{dx}\Bigg[\left(\sum_{j=1}^{N_z}q_j\frac{d\Phi_j}{dx}\right)\left(s\sum_{j=1}^{N_x}r_j\frac{d\Psi_j}{dx}+\frac{1}{2}\sum_{i=1}^{N_z}\sum_{j=1}^{N_z}q_iq_j\frac{d\Phi_j}{dx}\frac{d\Phi_i}{dx}\right)\\
&-\chi_g^2\left(\sum_{j=1}^{N_z}q_j\frac{d\Phi_j}{dx}\right)\frac{d^2}{dx^2}\left(s\sum_{j=1}^{N_x}r_j\frac{d\Psi_j}{dx}+\frac{1}{2}\sum_{i=1}^{N_z}\sum_{j=1}^{N_z}q_iq_j\frac{d\Phi_j}{dx}\frac{d\Phi_i}{dx}\right)\\
&+\eta\left(\sum_{j=1}^{N_z}q_j\frac{d\Phi_j}{dx}\right)\left(s\sum_{j=1}^{N_x}\frac{dr_j}{dt}\frac{d\Psi_j}{dx}+\sum_{i=1}^{N_z}\sum_{j=1}^{N_z}q_i\frac{dq_j}{dt}\frac{d\Phi_j}{dx}\frac{d\Phi_i}{dx}\right)\\
&-\chi_g^2\eta\left(\sum_{j=1}^{N_z}q_j\frac{d\Phi_j}{dx}\right)\frac{d^2}{dx^2}\left(s\sum_{j=1}^{N_x}\frac{dr_j}{dt}\frac{d\Psi_j}{dx}+\sum_{i=1}^{N_z}\sum_{j=1}^{N_z}q_i\frac{dq_j}{dt}\frac{d\Phi_j}{dx}\frac{d\Phi_i}{dx}\right)\\
&+\frac{s\chi_n^2}{r_A}\left(\sum_{j=1}^{N_z}q_j\frac{d\Phi_j}{dx}\right)\left(\sum_{j=1}^{N_x}\frac{d^2r_j}{dt^2}\frac{d\Psi_j}{dx}+2\kappa_{BK}\sqrt{\bar{M}}U\sum_{j=1}^{N_x}\frac{dr_j}{dt}\frac{d^2\Psi_j}{dx^2}+\kappa_{BK}^2U^2\sum_{j=1}^{N_x}r_j\frac{d^3\Psi_j}{dx^3}\right)\Bigg]\Bigg\}dx\\
&+\frac{r_A\chi_n^2}{s^2}\int_0^1\Bigg\{\Phi_k\frac{d^3}{dx^3}\Bigg[\left(\sum_{j=1}^{N_z}q_j\frac{d\Phi_j}{dx}\right)\left(s\sum_{j=1}^{N_x}r_j\frac{d\Psi_j}{dx}+\frac{1}{2}\sum_{i=1}^{N_z}\sum_{j=1}^{N_z}q_iq_j\frac{d\Phi_j}{dx}\frac{d\Phi_i}{dx}\right)\\
&-\chi_g^2\left(\sum_{j=1}^{N_z}q_j\frac{d\Phi_j}{dx}\right)\frac{d^2}{dx^2}\left(s\sum_{j=1}^{N_x}r_j\frac{d\Psi_j}{dx}+\frac{1}{2}\sum_{i=1}^{N_z}\sum_{j=1}^{N_z}q_iq_j\frac{d\Phi_j}{dx}\frac{d\Phi_i}{dx}\right)\\
&+\eta\left(\sum_{j=1}^{N_z}q_j\frac{d\Phi_j}{dx}\right)\left(s\sum_{j=1}^{N_x}\frac{dr_j}{dt}\frac{d\Psi_j}{dx}+\sum_{i=1}^{N_z}\sum_{j=1}^{N_z}q_i\frac{dq_j}{dt}\frac{d\Phi_j}{dx}\frac{d\Phi_i}{dx}\right)\\
&-\eta\chi_g^2\left(\sum_{j=1}^{N_z}q_j\frac{d\Phi_j}{dx}\right)\frac{d^2}{dx^2}\left(s\sum_{j=1}^{N_x}\frac{dr_j}{dt}\frac{d\Psi_j}{dx}+\sum_{i=1}^{N_z}\sum_{j=1}^{N_z}q_i\frac{dq_j}{dt}\frac{d\Phi_j}{dx}\frac{d\Phi_i}{dx}\right)\\
&+\frac{s\chi_n^2}{r_A}\left(\sum_{j=1}^{N_z}q_j\frac{d\Phi_j}{dx}\right)\left(\sum_{j=1}^{N_x}\frac{d^2r_j}{dt^2}\frac{d\Psi_j}{dx}+2\kappa_{BK}\sqrt{\bar{M}}U\sum_{j=1}^{N_x}\frac{dr_j}{dt}\frac{d^2\Psi_j}{dx^2}+\kappa_{BK}^2U^2\sum_{j=1}^{N_x}r_j\frac{d^3\Psi_j}{dx^3}\right)\Bigg]\Bigg\}dx=0.
\end{aligned}
\tag{24}
$$

Asterisk notations are dropped for the sake of convenience. Equations (23) and (24) are simultaneously solved employing a direct time-integration scheme of solution for obtaining the nonlinear size-dependent motion characteristics of fluid-conveying tubes at nanoscales. As seen from the above equations, using the Galerkin approach, the partial differential equations of motion are reduced into a set of time-dependent ordinary equations. Then, a direct time-integration scheme is implemented to accurately solve this set of time-dependent equations. The direct time integration is performed by applying a variable step-size modified Rosenbrock approach. This approach gives the amplitude of motion of the nanotube in terms of time. It is worth pointing out that ten shape functions are considered for each displacement, resulting in a system of twenty shape functions.

4. Results and discussion

A nanofluid-conveying nanotube with length-to-diameter ratio L/d_{out}=20, thickness h=70.0 nm, outer radius R_{out} =230.0 nm, elasticity modulus E=610 MPa, density 1024 kg/m^3 and Poisson's ratio v=0.3 is considered. The non-dimensional parameters of the above-described nanosystem are as Kn=0.02, κ_{BK} =1.1595, $\bar{M}$ =0.4780, r_A= 4312.8662, $\chi_g = 0.03$ and $\chi_n = 0.09$. For all cases, which are studied in the following, it is supposed that ω/ω_1=1.0. In total, 20 degrees of freedom are considered (10 for w and 10 for u). The critical flow velocity corresponding to buckling is 4.7817.

Figure 2 shows the bifurcation behaviour of Poincaré sections of the viscoelastic nanotube conveying nanofluid flow for the transverse displacement at x=0.50 as well as the longitudinal displacement at x=0.65; the natural frequency and flow velocity are ω_1= 3.1201 and U = 4.70, respectively. The flow velocity is smaller than the critical velocity, leading to a subcritical bifurcation behaviour. It is found that period-1 motions govern the nonlinear behaviour of the nanofluid-conveying nanotube with viscoelastic properties for very small loading amplitudes. By further changing the loading amplitude, other motion types such as period-5, period-3 and period-2 are obtained for the viscoelastic system. Another important finding is that the viscoelastic nanoscale tube does not exhibit any chaotic motion at this flow velocity. For instance, the dynamical characteristics of the viscoelastic system of Fig. 2 at F_1=14.0 and F_1=40.2 are shown in Figs. 3 and 4, respectively. It is concluded that the motion type is period-3 and period-2 at F_1=14.0 and F_1=40.2, respectively.

Figure 5 depicts the subcritical bifurcation behaviour of Poincaré sections of the viscoelastic nanotube conveying nanofluid flow for the transverse displacement at x=0.50 and the longitudinal displacement at x=0.65; ω_1= 1.9306 and U = 4.75. Comparing Figs. 2 and

5 indicates that a slight increase in the flow velocity at nanoscales leads to a dramatic change in the subcritical bifurcation behaviour of viscoelastic nanotubes. Several chaotic regions are observed in Fig. 5 while there is no chaos in Fig. 4. The dynamical characteristics of the motion of the viscoelastic system of Fig. 5 at F_1=38.0 are depicted in Fig. 6; it is seen that the motion is periodic for this loading amplitude.

The supercritical bifurcation behaviour of Poincaré sections of the viscoelastic nanotube conveying nanofluid flow is plotted in Fig. 7 for the transverse motion at x=0.50 and the longitudinal motion at x=0.65; the natural frequency and flow velocity are as ω_1=2.0656 and U=4.80, respectively. It is found that the viscoelastic nanosystem exhibits a variety of motions at this flow velocity. Compared to the subcritical response plotted in Fig. 5, the first chaotic region of the supercritical behaviour of Fig. 7 starts at a lower loading amplitude. To give more details, the dynamical characteristics of the size-dependent motion of the viscoelastic system of Fig. 7 at F_1=28.0 are depicted in Fig. 8; both motions along x and z axes are highly chaotic for this loading amplitude. In addition, Fig. 9 shows the dynamical characteristics of the period-3 motion of the system of Fig. 7 at F_1=58.0.

Figure 10 depicts the supercritical bifurcation behaviour of Poincaré sections of the viscoelastic nanotube conveying nanofluid flow for the transverse motion at x=0.50 and the axial motion at x=0.65; ω_1= 3.9731 and U = 4.85. The dynamical characteristics of the chaotic motion of the system of this figure at F_1=36.0 are also shown in Fig. 11. Comparing Figs. 7 and 10 indicates that the number of chaotic regions for the coupled motion is significantly reduced by a small increase in the flow velocity after the critical point corresponding to buckling.

In general, it is observed that the number of chaotic regions is greatly affected by the flow velocity. In the subcritical regime, increasing the flow velocity increases the number of chaotic regions whereas increasing the flow velocity in the supercritical regime reduces this number. The mechanics reason for these phenomena is that when the flow velocity increases in the subcritical regime, the nanotube approaches the instability state, which is determined by the critical speed. By contrast, the nanotube approaches this state by decreasing the flow velocity in the supercritical regime.

In order to compare various scale-dependent theories involving strain gradient, nonlocal, classical and nonlocal strain gradient, Figs. 12 and 13 are plotted. The results of the nonlocal model are shown in Fig. 12(a) while the results of the strain gradient model are illustrated in Fig. 12(b). Moreover, the NSGT and classical theory (CT) are compared in Fig. 13. For the nonlocal, strain gradient, NSGT and CT, the size parameters are set to $(\chi_n \neq 0, \chi_g = 0)$, $(\chi_n = 0, \chi_g \neq 0)$, $(\chi_n \neq 0, \chi_g \neq 0)$ and $(\chi_n = 0, \chi_g = 0)$, respectively. It is found that the critical fluid velocity decreases with increasing χ_n while χ_g has an increasing effect on the critical velocity. This is rooted in the fact that increasing χ_n leads to a reduction in the structural stiffness whereas χ_g has an increasing effect on the structural stiffness at nanoscales.

5. Conclusions

A coupled nonlinear NSGT-based model was proposed for the bifurcation behaviour of nanofluid-conveying nanotubes with viscoelastic properties. Size influences on the bifurcation behaviour of the nanotube were incorporated via a modified viscoelastic model

of nanobeams. Furthermore, for incorporating size influences on the nanofluid, the Beskok-Karniadakis theory was used. Also, nonlinear strain-displacement relations were employed for modelling the geometric nonlinearity. The coupled differential equations of axial and transverse motions incorporating the internal energy loss were derived via the Kelvin-Voigt model and Hamilton's principle. Finally, the Galerkin procedure and a direct time-integration scheme were applied for extracting the bifurcation characteristics of the viscoelastic nanosystem. It was concluded that the bifurcation behaviour is very sensitive to the flow velocity. In both supercritical and subcritical regimes, chaotic motions were found for the viscoelastic nanotube. The number of chaotic regions depends on the flow velocity. In the subcritical regime, the number of chaotic regions increases with increasing flow velocity whereas this number reduces with increasing flow velocity in the supercritical regime.

Appendix A. Verification study

The critical nanofluid velocity is verified in the following by comparing it with that obtained in the literature using the NSGT-based beam model. An analytical solution for the critical fluid velocity of nanotubes conveying fluid was presented by Li et al. [36]. Neglecting large deflections, slip boundary conditions and external force, Eqs. (18) and (19) are reduced to the following equation

$$EI\left(1-\ell_g^2\nabla^2\right)\frac{\partial^4 w}{\partial x^4}+\left(1-\left(e_0\ell_n\right)^2\nabla^2\right)\times \left[\left(m+M\right)\frac{\partial^2 w}{\partial t^2}+2MU\frac{\partial^2 w}{\partial x\partial t}+MU^2\frac{\partial^2 w}{\partial x^2}\right]=0. \tag{A1}$$

To obtain the critical fluid velocity, one can write

$$w = \sum_{k=1}^{\infty} W_k \sin\left(\frac{k\pi x}{L}\right). \tag{A2}$$

Substituting Eq. (A2) into Eq. (A1), the critical velocity for k=1 is obtained as

$$U_{cr} = \sqrt{\frac{\pi^2 EI\left(L^2 + \pi^2 \ell_g^2\right)}{ML^2\left[L^2 + \pi^2\left(e_0 \ell_n\right)^2\right]}}. \tag{A3}$$

It should be noted that the flow-profile-modification factor is ignored in this analysis. The above relation for the critical velocity is the same as that obtained by Li et al. [36] when the flow-profile-modification factor is zero.

References

[1] Abdelgawad M, Wheeler AR. Low-cost, rapid-prototyping of digital microfluidics devices. Microfluidics and nanofluidics. 2008;4:349.
[2] Li Z, He Y, Lei J, Han S, Guo S, Liu D. Experimental investigation on size-dependent higher-mode vibration of cantilever microbeams. Microsystem Technologies. 2018;DOI: https://doi.org/10.1007/s00542-018-4244-0.
[3] Asemi SR, Farajpour A. Vibration characteristics of double-piezoelectric-nanoplate-systems. IET Micro & Nano Letters. 2014;9:280-5.
[4] Ghayesh MH, Farokhi H, Gholipour A. Vibration analysis of geometrically imperfect three-layered shear-deformable microbeams. International Journal of Mechanical Sciences. 2017;122:370-83.
[5] Farokhi H, Ghayesh MH, Hussain S. Large-amplitude dynamical behaviour of microcantilevers. International Journal of Engineering Science. 2016;106:29-41.
[6] Ghayesh MH. Dynamics of functionally graded viscoelastic microbeams. International Journal of Engineering Science. 2018;124:115-31.
[7] Mohammadi M, Farajpour A, Goodarzi M. Numerical study of the effect of shear in-plane load on the vibration analysis of graphene sheet embedded in an elastic medium. Computational Materials Science. 2014;82:510-20.
[8] Rashvand K, Rezazadeh G, Mobki H, Ghayesh MH. On the size-dependent behavior of a capacitive circular micro-plate considering the variable length-scale parameter. International Journal of Mechanical Sciences. 2013;77:333-42.
[9] Farokhi H, Ghayesh MH. Nonlinear resonant response of imperfect extensible Timoshenko microbeams. International Journal of Mechanics and Materials in Design. 2017;13:43-55.
[10] Ghayesh MH, Farokhi H, Hussain S. Viscoelastically coupled size-dependent dynamics of microbeams. International Journal of Engineering Science. 2016;109:243-55.
[11] Farokhi H, Ghayesh MH, Gholipour A, Hussain S. Motion characteristics of bilayered extensible Timoshenko microbeams. International Journal of Engineering Science. 2017;112:1-17.
[12] Asemi SR, Farajpour A. Decoupling the nonlocal elasticity equations for thermo-mechanical vibration of circular graphene sheets including surface effects. Physica E: Low-Dimensional Systems and Nanostructures. 2014;60:80-90.

[13] Aydogdu M. A nonlocal rod model for axial vibration of double-walled carbon nanotubes including axial van der Waals force effects. Journal of Vibration and Control. 2015;21:3132-54.
[14] Aydogdu M, Elishakoff I. On the vibration of nanorods restrained by a linear spring in-span. Mechanics Research Communications. 2014;57:90-6.
[15] Reddy J. Nonlocal theories for bending, buckling and vibration of beams. International Journal of Engineering Science. 2007;45:288-307.
[16] Reddy J, Pang S. Nonlocal continuum theories of beams for the analysis of carbon nanotubes. Journal of Applied Physics. 2008;103:023511.
[17] Bahaadini R, Hosseini M. Nonlocal divergence and flutter instability analysis of embedded fluid-conveying carbon nanotube under magnetic field. Microfluidics and nanofluidics. 2016;20:108.
[18] Ma H, Gao X-L, Reddy J. A microstructure-dependent Timoshenko beam model based on a modified couple stress theory. Journal of the Mechanics and Physics of Solids. 2008;56:3379-91.
[19] Ghayesh MH, Farokhi H, Farajpour A. Chaotic oscillations of viscoelastic microtubes conveying pulsatile fluid. Microfluidics and Nanofluidics. 2018;22:72.
[20] Xia W, Wang L. Microfluid-induced vibration and stability of structures modeled as microscale pipes conveying fluid based on non-classical Timoshenko beam theory. Microfluidics and nanofluidics. 2010;9:955-62.
[21] Deng J, Liu Y, Liu W. Size-dependent vibration analysis of multi-span functionally graded material micropipes conveying fluid using a hybrid method. Microfluidics and nanofluidics. 2017;21:133.
[22] Dehrouyeh-Semnani AM, Nikkhah-Bahrami M, Yazdi MRH. On nonlinear stability of fluid-conveying imperfect micropipes. International Journal of Engineering Science. 2017;120:254-71.
[23] Li L, Hu Y. Buckling analysis of size-dependent nonlinear beams based on a nonlocal strain gradient theory. International Journal of Engineering Science. 2015;97:84-94.
[24] Şimşek M. Nonlinear free vibration of a functionally graded nanobeam using nonlocal strain gradient theory and a novel Hamiltonian approach. International Journal of Engineering Science. 2016;105:12-27.
[25] Farajpour M, Shahidi A, Tabataba'i-Nasab F, Farajpour A. Vibration of initially stressed carbon nanotubes under magneto-thermal environment for nanoparticle delivery via higher-order nonlocal strain gradient theory. The European Physical Journal Plus. 2018;133:219.
[26] Rahmati M, Khodaei S. Nonlocal vibration and instability analysis of carbon nanotubes conveying fluid considering the influences of nanoflow and non-uniform velocity profile. Microfluidics and nanofluidics. 2018;22:117.
[27] Hadi A, Nejad MZ, Hosseini M. Vibrations of three-dimensionally graded nanobeams. International Journal of Engineering Science. 2018;128:12-23.
[28] Li L, Hu Y, Ling L. Wave propagation in viscoelastic single-walled carbon nanotubes with surface effect under magnetic field based on nonlocal strain gradient theory. Physica E: Low-Dimensional Systems and Nanostructures. 2016;75:118-24.
[29] Sudak L. Column buckling of multiwalled carbon nanotubes using nonlocal continuum mechanics. Journal of applied physics. 2003;94:7281-7.
[30] Murmu T, Pradhan S. Thermo-mechanical vibration of a single-walled carbon nanotube embedded in an elastic medium based on nonlocal elasticity theory. Computational Materials Science. 2009;46:854-9.
[31] Farajpour A, Rastgoo A. Influence of carbon nanotubes on the buckling of microtubule bundles in viscoelastic cytoplasm using nonlocal strain gradient theory. Results in physics. 2017;7:1367-75.
[32] Farajpour MR, Shahidi A, Farajpour A. Resonant frequency tuning of nanobeams by piezoelectric nanowires under thermo-electro-magnetic field: a theoretical study. Micro & Nano Letters. 2018;13:1627 – 32.
[33] Setoodeh A, Khosrownejad M, Malekzadeh P. Exact nonlocal solution for postbuckling of single-walled carbon nanotubes. Physica E: Low-dimensional Systems and Nanostructures. 2011;43:1730-7.

[34] Ghayesh MH, Farajpour A. Nonlinear mechanics of nanoscale tubes via nonlocal strain gradient theory. International Journal of Engineering Science. 2018;129:84-95.
[35] Amiri A, Talebitooti R, Li L. Wave propagation in viscous-fluid-conveying piezoelectric nanotubes considering surface stress effects and Knudsen number based on nonlocal strain gradient theory. The European Physical Journal Plus. 2018;133:252.
[36] Li L, Hu Y, Li X, Ling L. Size-dependent effects on critical flow velocity of fluid-conveying microtubes via nonlocal strain gradient theory. Microfluidics and nanofluidics. 2016;20:76.
[37] Li L, Hu Y. Wave propagation in fluid-conveying viscoelastic carbon nanotubes based on nonlocal strain gradient theory. Computational Materials Science. 2016;112:282-8.
[38] Ghayesh MH, Farajpour A. Nonlinear coupled mechanics of nanotubes incorporating both nonlocal and strain gradient effects. Mechanics of Advanced Materials and Structures. 2018;doi: 10.1080/15376494.2018.1473537:1-10.
[39] Farajpour A, Ghayesh MH, Farokhi H. Large-amplitude coupled scale-dependent behaviour of geometrically imperfect NSGT nanotubes. International Journal of Mechanical Sciences. 2019;150:510-25.
[40] Zhu X, Li L. On longitudinal dynamics of nanorods. International Journal of Engineering Science. 2017;120:129-45.
[41] Wang L. Size-dependent vibration characteristics of fluid-conveying microtubes. Journal of Fluids and Structures. 2010;26:675-84.
[42] Lee H-L, Chang W-J. Free transverse vibration of the fluid-conveying single-walled carbon nanotube using nonlocal elastic theory. Journal of Applied Physics. 2008;103:024302.
[43] Soltani P, Taherian M, Farshidianfar A. Vibration and instability of a viscous-fluid-conveying single-walled carbon nanotube embedded in a visco-elastic medium. Journal of Physics D: Applied Physics. 2010;43:425401.
[44] Zeighampour H, Beni YT. Size-dependent vibration of fluid-conveying double-walled carbon nanotubes using couple stress shell theory. Physica E: Low-Dimensional Systems and Nanostructures. 2014;61:28-39.
[45] Zhen Y-X, Fang B, Tang Y. Thermal–mechanical vibration and instability analysis of fluid-conveying double walled carbon nanotubes embedded in visco-elastic medium. Physica E: Low-dimensional Systems and Nanostructures. 2011;44:379-85.
[46] Maraghi ZK, Arani AG, Kolahchi R, Amir S, Bagheri M. Nonlocal vibration and instability of embedded DWBNNT conveying viscose fluid. Composites Part B: Engineering. 2013;45:423-32.
[47] Liang F, Su Y. Stability analysis of a single-walled carbon nanotube conveying pulsating and viscous fluid with nonlocal effect. Applied Mathematical Modelling. 2013;37:6821-8.
[48] Askari H, Esmailzadeh E. Forced vibration of fluid conveying carbon nanotubes considering thermal effect and nonlinear foundations. Composites Part B: Engineering. 2017;113:31-43.
[49] Ghasemi A, Dardel M, Ghasemi MH, Barzegari MM. Analytical analysis of buckling and post-buckling of fluid conveying multi-walled carbon nanotubes. Applied Mathematical Modelling. 2013;37:4972-92.
[50] Oveissi S, Toghraie D, Eftekhari SA. Longitudinal vibration and stability analysis of carbon nanotubes conveying viscous fluid. Physica E: Low-dimensional Systems and Nanostructures. 2016;83:275-83.
[51] Farajpour A, Rastgoo A, Farajpour M. Nonlinear buckling analysis of magneto-electro-elastic CNT-MT hybrid nanoshells based on the nonlocal continuum mechanics. Composite Structures. 2017;180:179-91.
[52] Gholipour A, Ghayesh MH, Zander A. Nonlinear biomechanics of bifurcated atherosclerotic coronary arteries. International Journal of Engineering Science. 2018;133:60-83.
[53] Gholipour A, Ghayesh MH, Zander A, Mahajan R. Three-dimensional biomechanics of coronary arteries. International Journal of Engineering Science. 2018;130:93-114.
[54] Lim C, Zhang G, Reddy J. A higher-order nonlocal elasticity and strain gradient theory and its applications in wave propagation. Journal of the Mechanics and Physics of Solids. 2015;78:298-313.

[55] Farajpour A, Ghayesh MH, Farokhi H. A review on the mechanics of nanostructures. International Journal of Engineering Science. 2018;133:231-63.
[56] Zhu X, Li L. Closed form solution for a nonlocal strain gradient rod in tension. International Journal of Engineering Science. 2017;119:16-28.
[57] Farajpour A, Rastgoo A, Mohammadi M. Vibration, buckling and smart control of microtubules using piezoelectric nanoshells under electric voltage in thermal environment. Physica B: Condensed Matter. 2017;509:100-14.
[58] Li L, Tang H, Hu Y. The effect of thickness on the mechanics of nanobeams. International Journal of Engineering Science. 2018;123:81-91.
[59] Tang H, Li L, Hu Y. Coupling effect of thickness and shear deformation on size-dependent bending of micro/nano-scale porous beams. Applied Mathematical Modelling. 2019;66:527-47.
[60] Deng W, Li L, Hu Y, Wang X, Li X. Thermoelastic damping of graphene nanobeams by considering the size effects of nanostructure and heat conduction. Journal of Thermal Stresses. 2018;41:1182-200.
[61] Beskok A, Karniadakis GE. Report: a model for flows in channels, pipes, and ducts at micro and nano scales. Microscale Thermophysical Engineering. 1999;3:43-77.

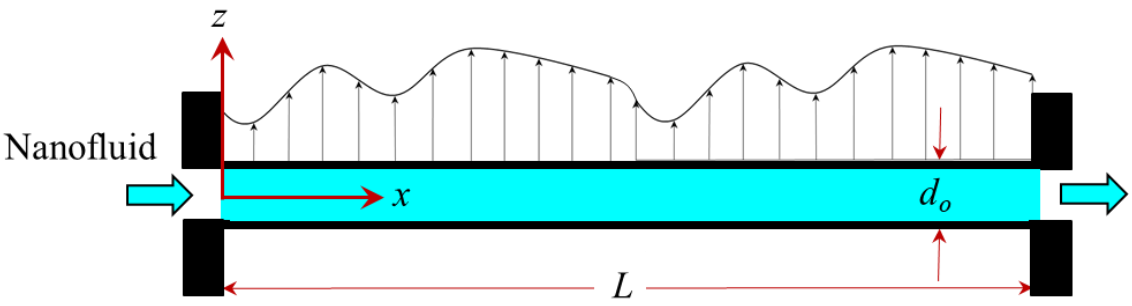

Fig. 1. A nanofluid-conveying nanotube under distributed excitation loading.

(a)

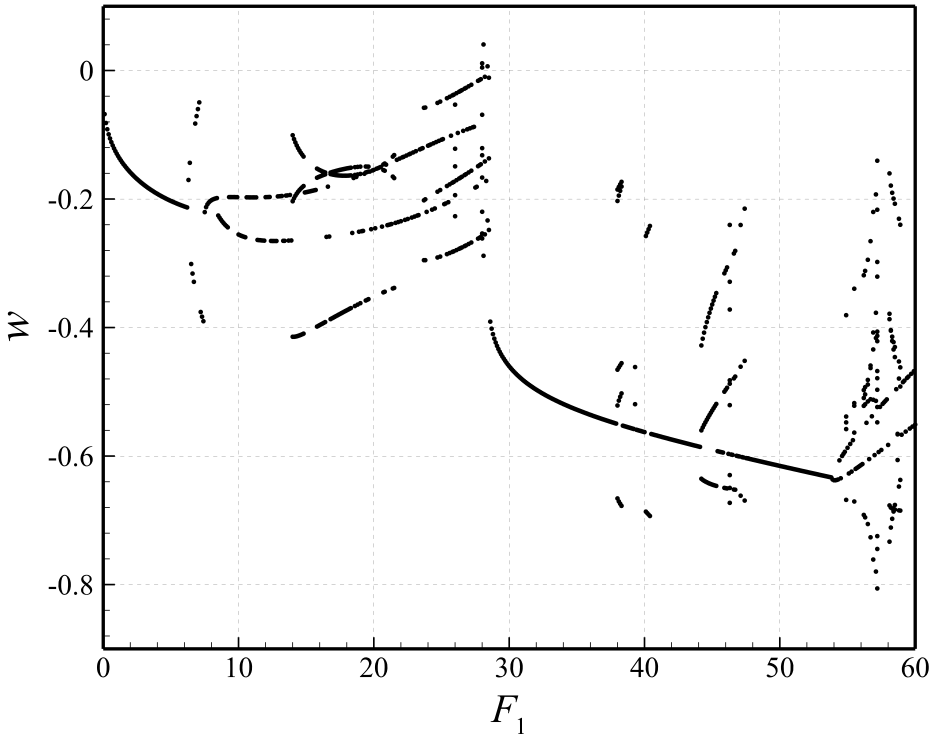

(b)

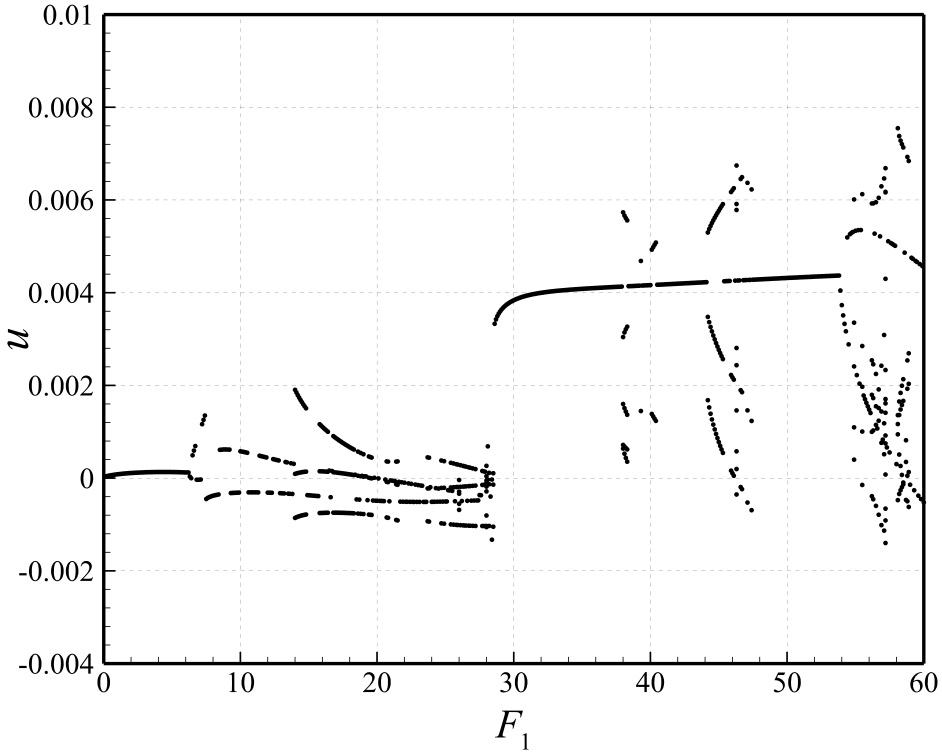

Figure 2: Subcritical bifurcation diagrams of Poincaré sections of the viscoelastic nanotube conveying nanofluid flow: (a) displacement along transverse axis at *x*=0.50; (b) displacement along longitudinal axis at *x*=0.65.

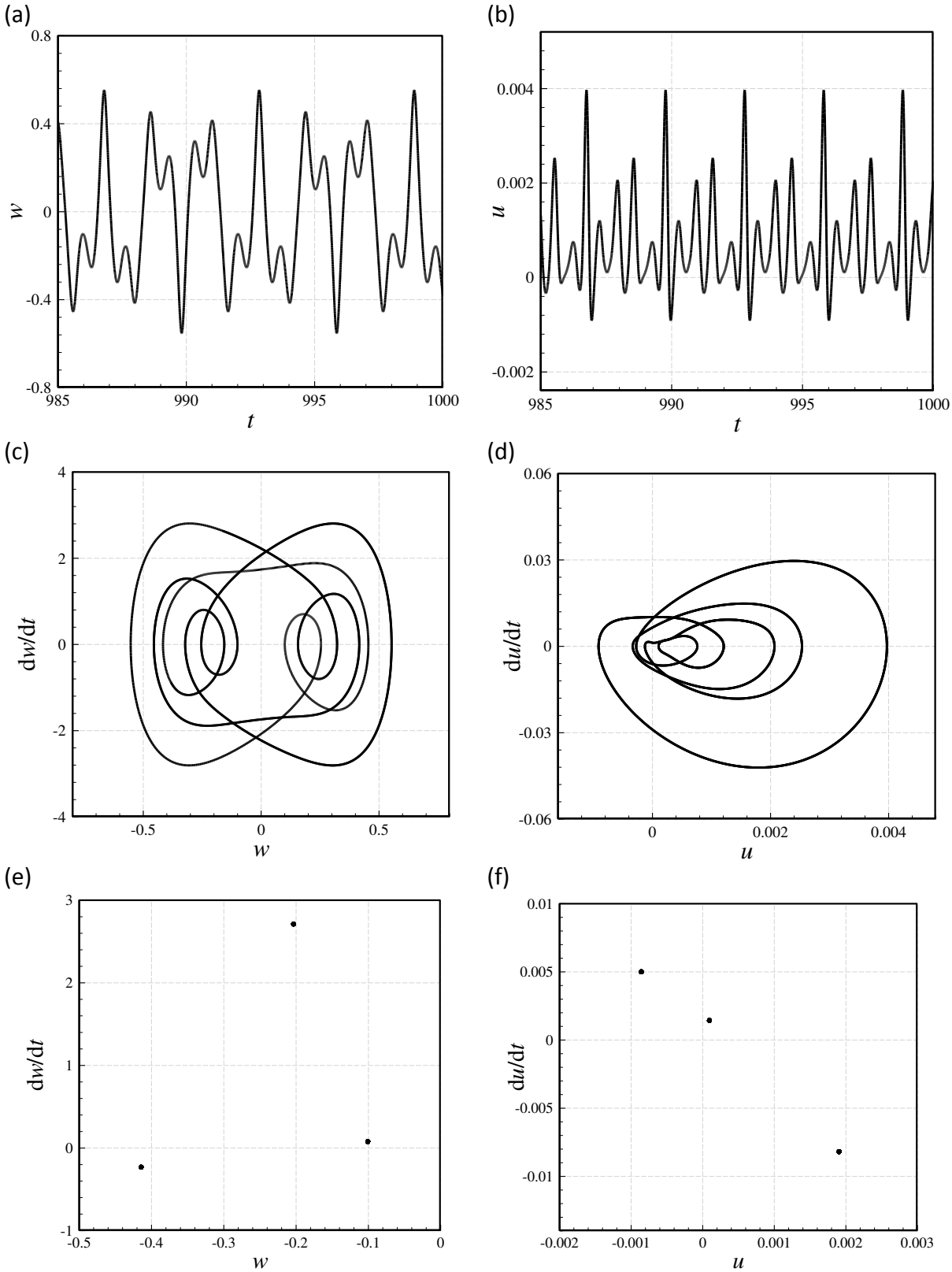

Figure 3: Dynamical characteristics of the period-3 motion of the nanosystem of Fig. 2 at F_1=14.0: time histories of (a) w (at x=0.5) and (b) u (at x=0.65); phase-plane plots of (c) w (at x=0.5) and (d) u (at x=0.65); Poincaré plots of (e) w (at x=0.5) and (f) u (at x=0.65).

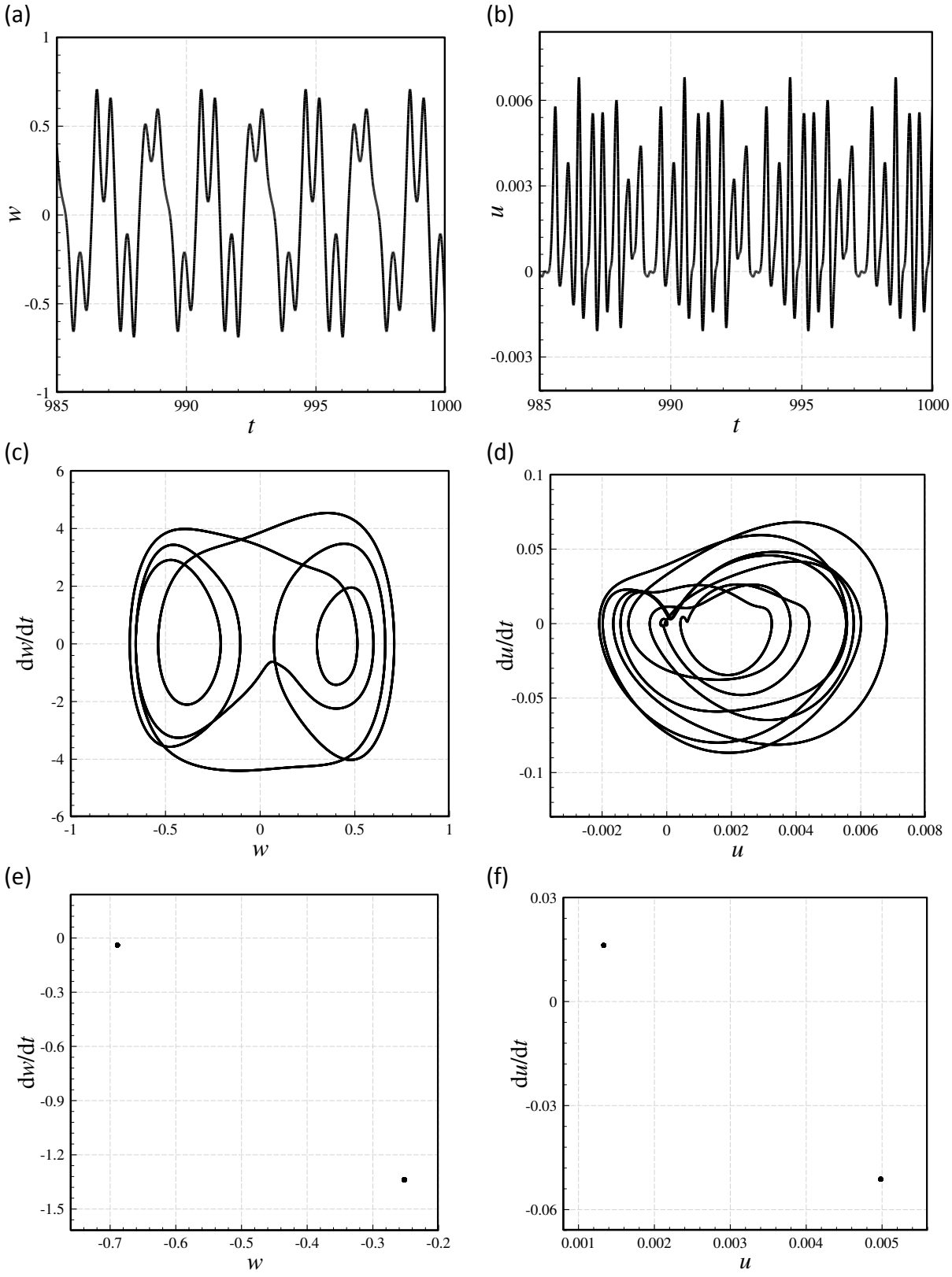

Figure 4: Dynamical characteristics of the coupled period-2 motions of the nanosystem of Fig. 2 at F_1=40.2: time histories of (a) w (at x=0.5) and (b) u (at x=0.65); phase-plane plots of (c) w (at x=0.5) and (d) u (at x=0.65); Poincaré plots of (e) w (at x=0.5) and (f) u (at x=0.65).

(a)

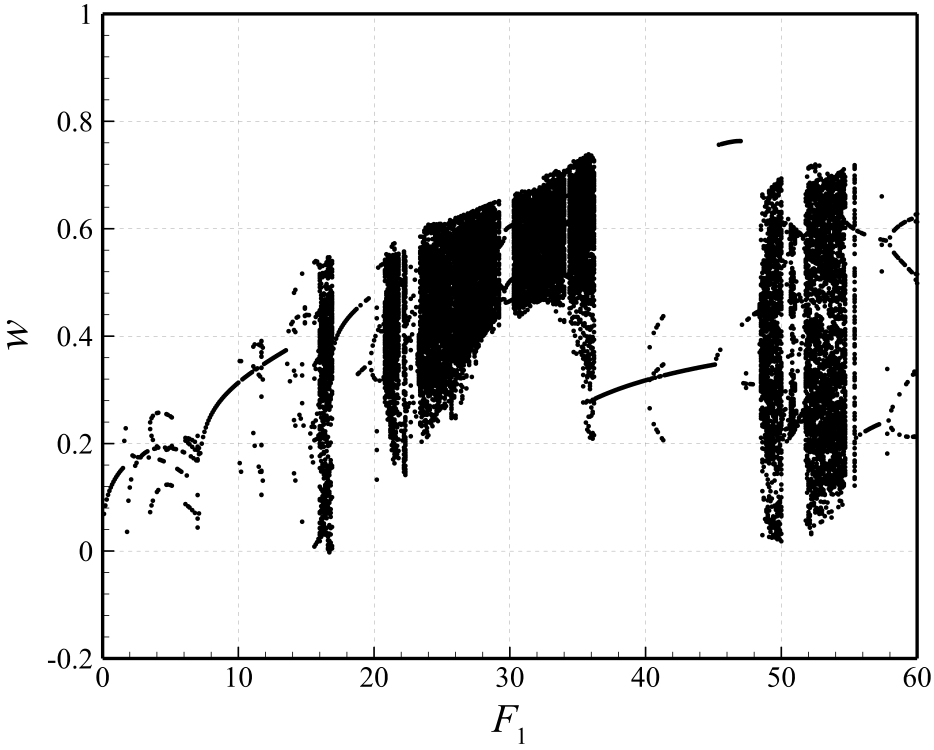

(b)

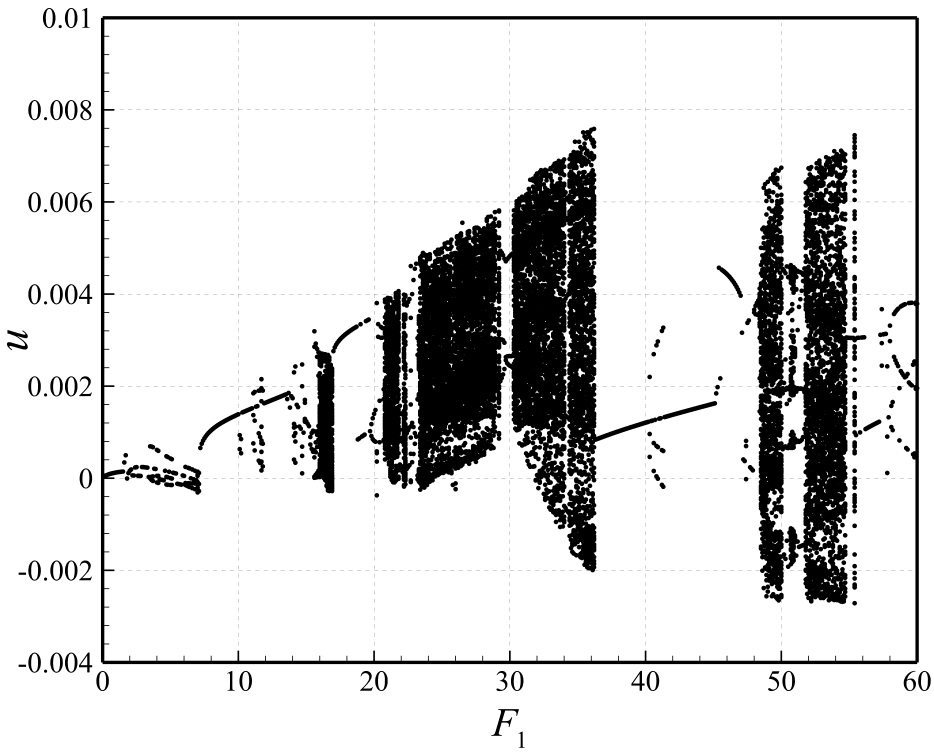

Figure 5: Subcritical bifurcation diagrams of Poincaré sections of the viscoelastic nanotube conveying nanofluid flow: (a) displacement along transverse axis at *x*=0.50; (b) displacement along longitudinal axis at *x*=0.65.

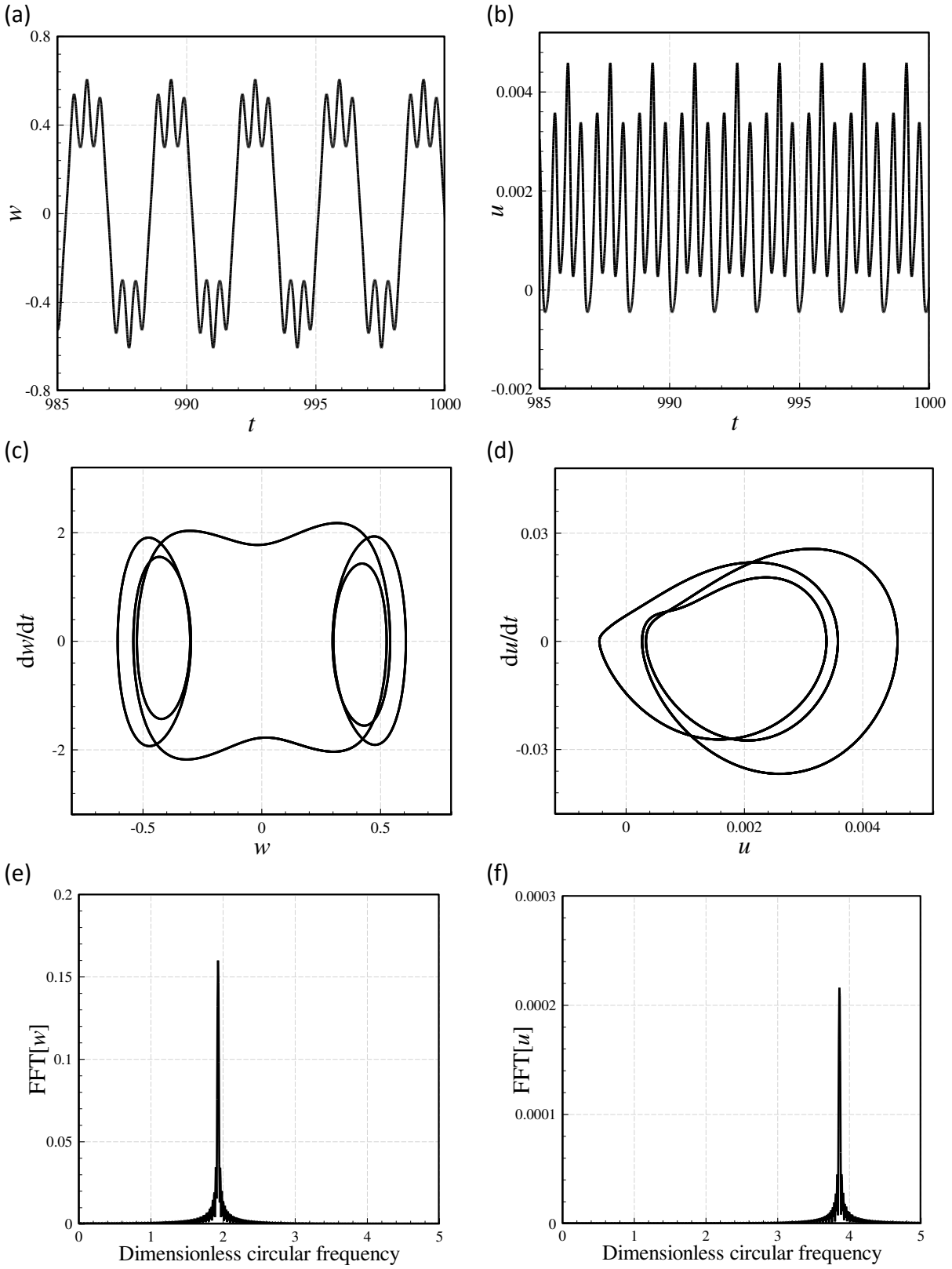

Figure 6: Dynamical characteristics of the periodic motion of the nanosystem of Fig. 5 at F_1=38.0: time histories of (a) w (at x=0.5) and (b) u (at x=0.65); phase-plane plots of (c) w (at x=0.5) and (d) u (at x=0.65); FFTs of (e) w (at x=0.5) and (f) u (at x=0.65).

(a)

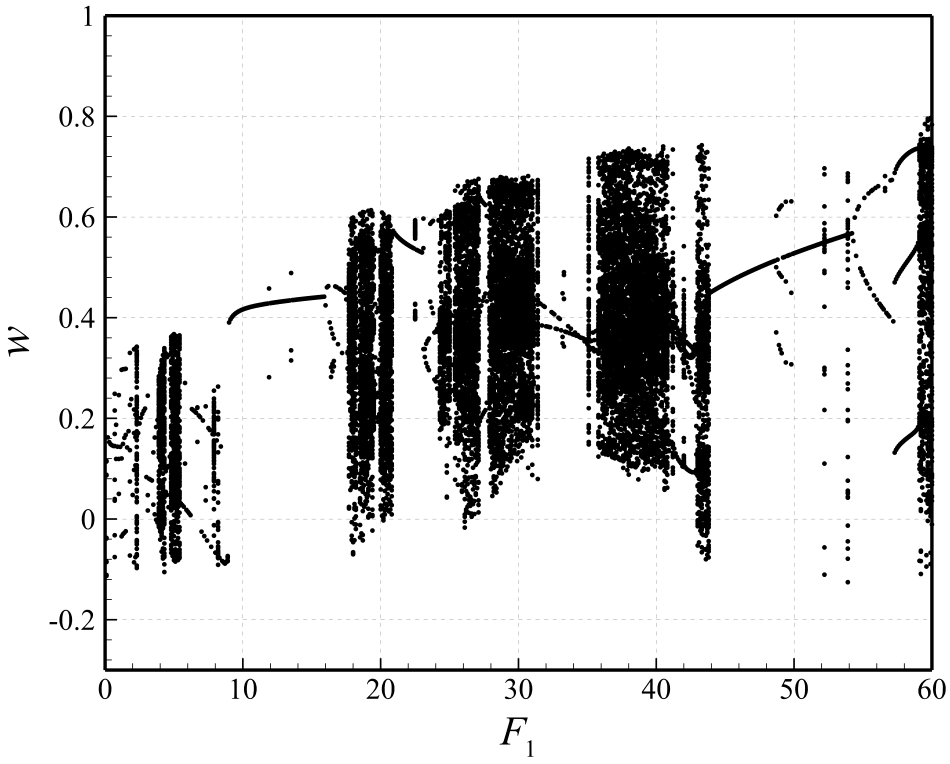

(b)

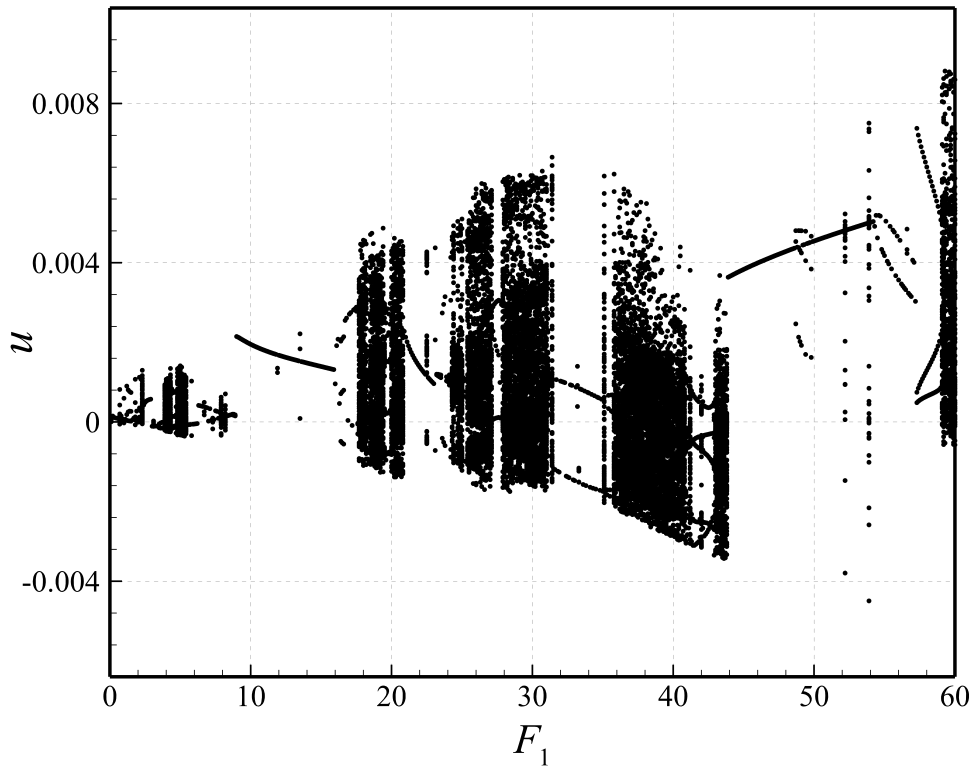

Figure 7: Supercritical bifurcation plots of Poincaré sections of the viscoelastic nanotube conveying nanofluid flow: (a) displacement along transverse axis at *x*=0.50; (b) displacement along longitudinal axis at *x*=0.65.

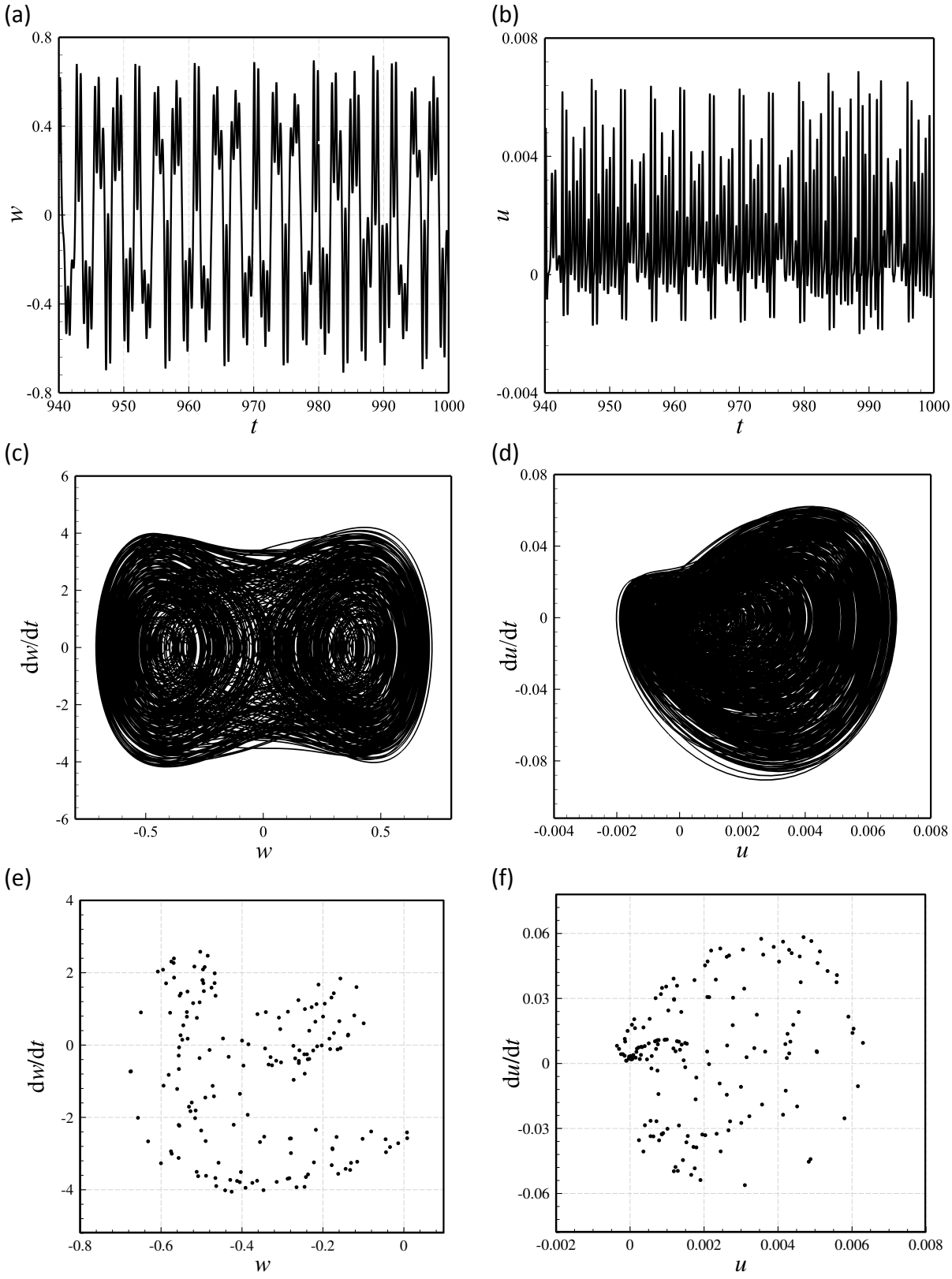

Figure 8: Dynamical characteristics of the chaotic motion of the nanosystem of Fig. 7 at F_1=28.0: time histories of (a) w (at x=0.5) and (b) u (at x=0.65); phase-plane plots of (c) w (at x=0.5) and (d) u (at x=0.65); Poincaré plots of (e) w (at x=0.5) and (f) u (at x=0.65).

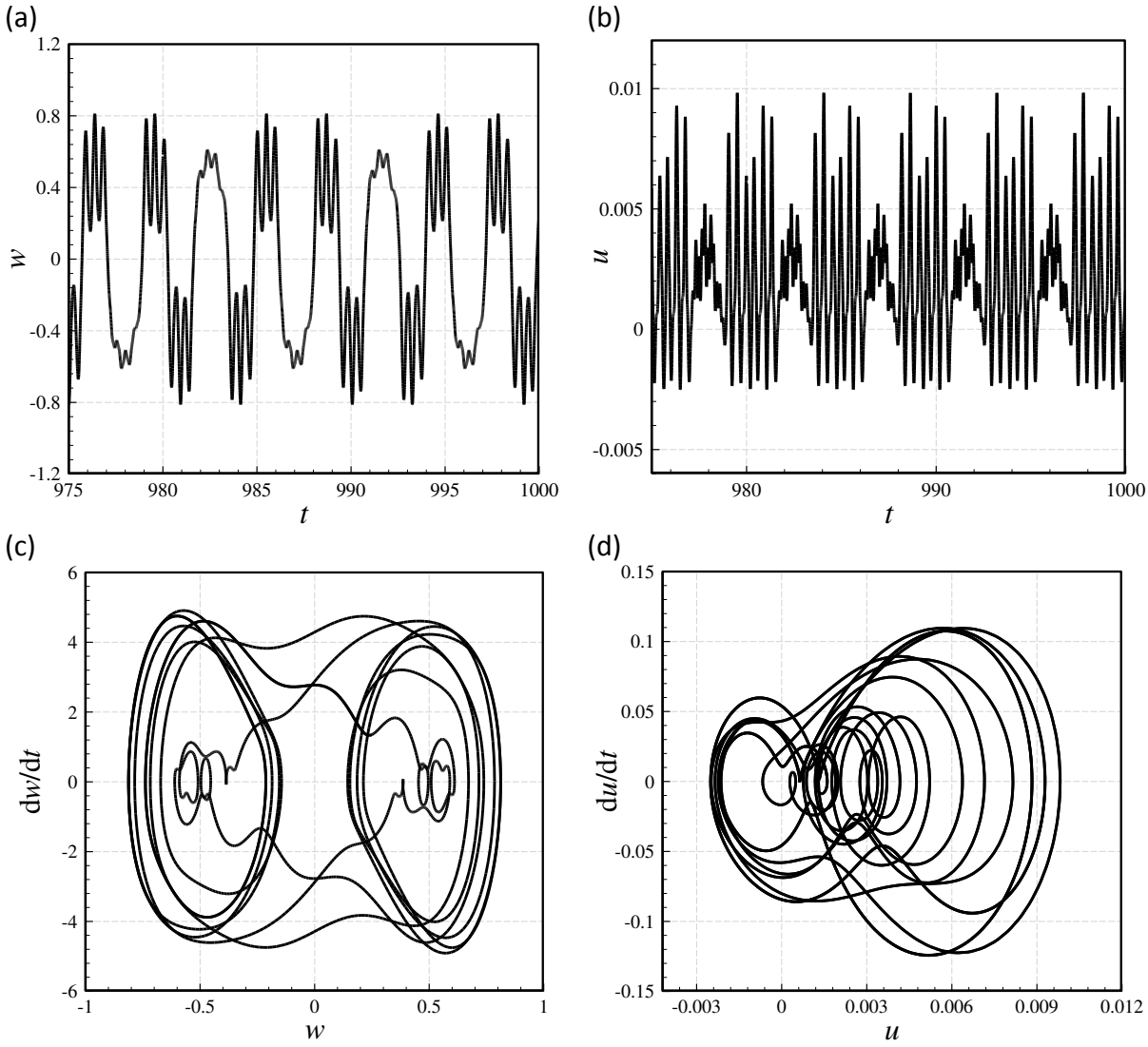

Figure 9: Dynamical characteristics of the period-3 motion of the nanosystem of Fig. 7 at F_1=58.0: time histories of (a) w (at x=0.5) and (b) u (at x=0.65); phase-plane plots of (c) w (at x=0.5) and (d) u (at x=0.65).

(a)

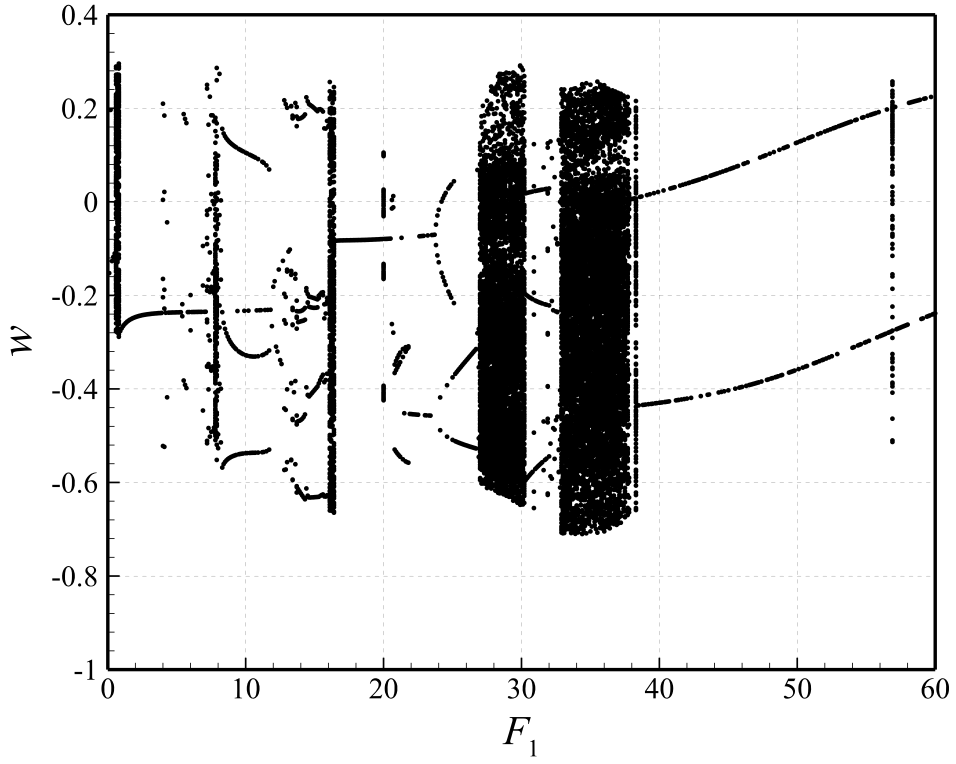

(b)

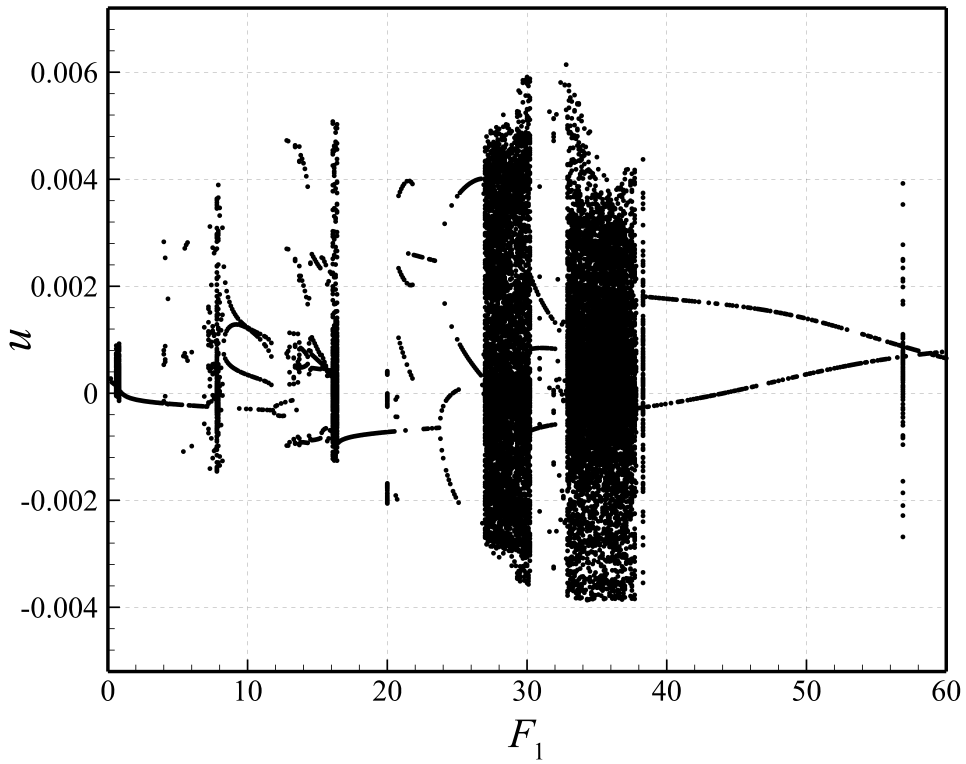

Figure 10: Supercritical bifurcation plots of Poincaré sections of the viscoelastic nanotube conveying nanofluid flow: (a) displacement along transverse axis at *x*=0.50; (b) displacement along longitudinal axis at *x*=0.65.

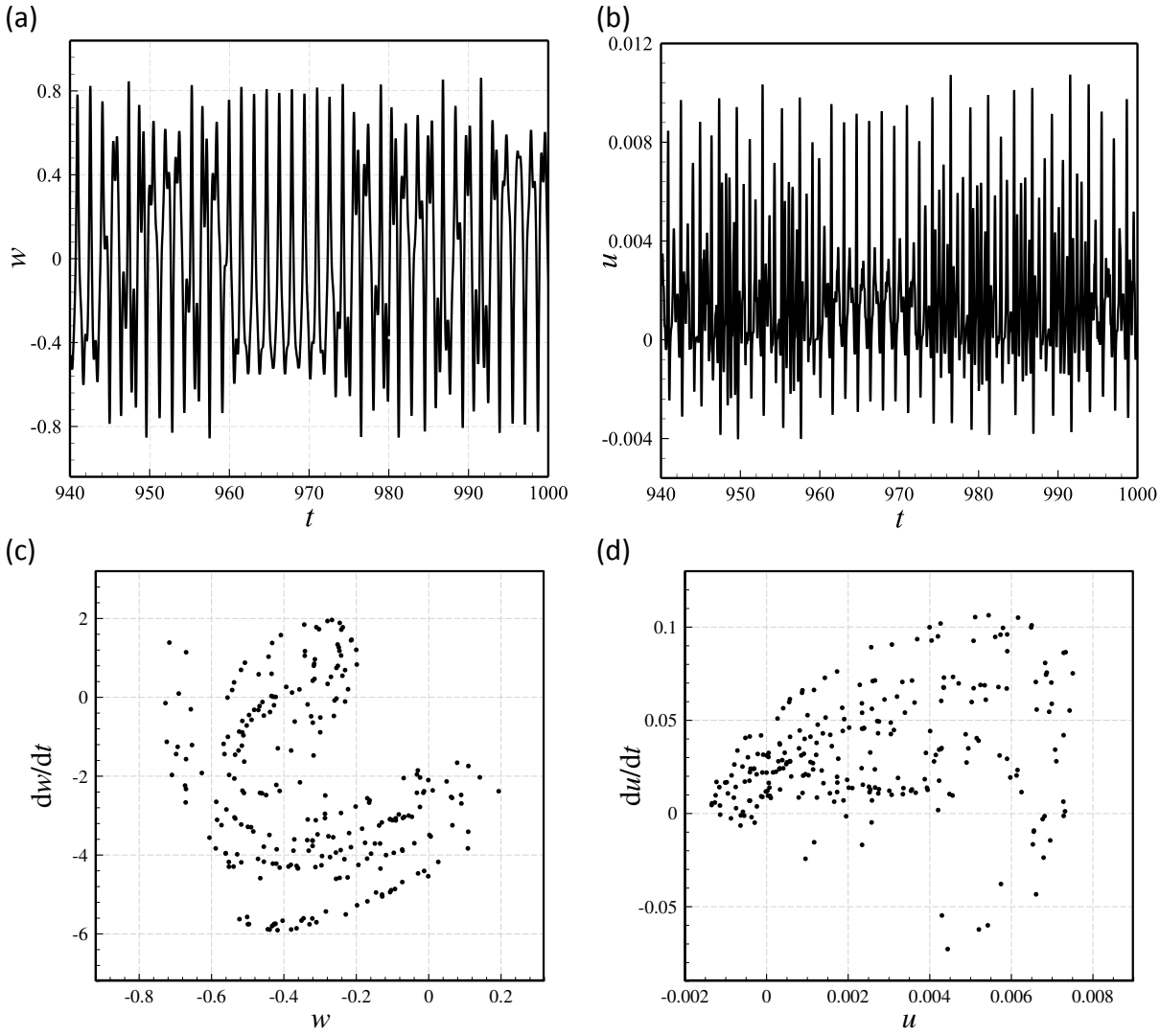

Figure 11: Dynamical characteristics of the chaotic motion of the nanosystem of Fig. 10 at F_1=36.0: time histories of (a) w (at x=0.5) and (b) u (at x=0.65); Poincaré plots of (c) w (at x=0.5) and (d) u (at x=0.65).

(a)

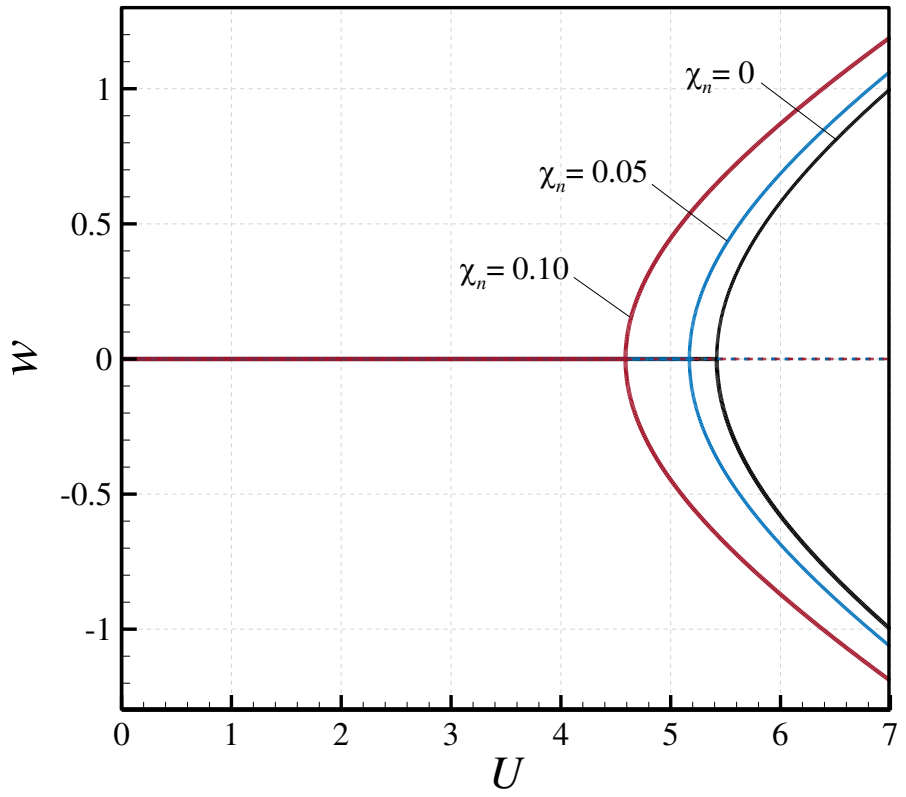

(b)

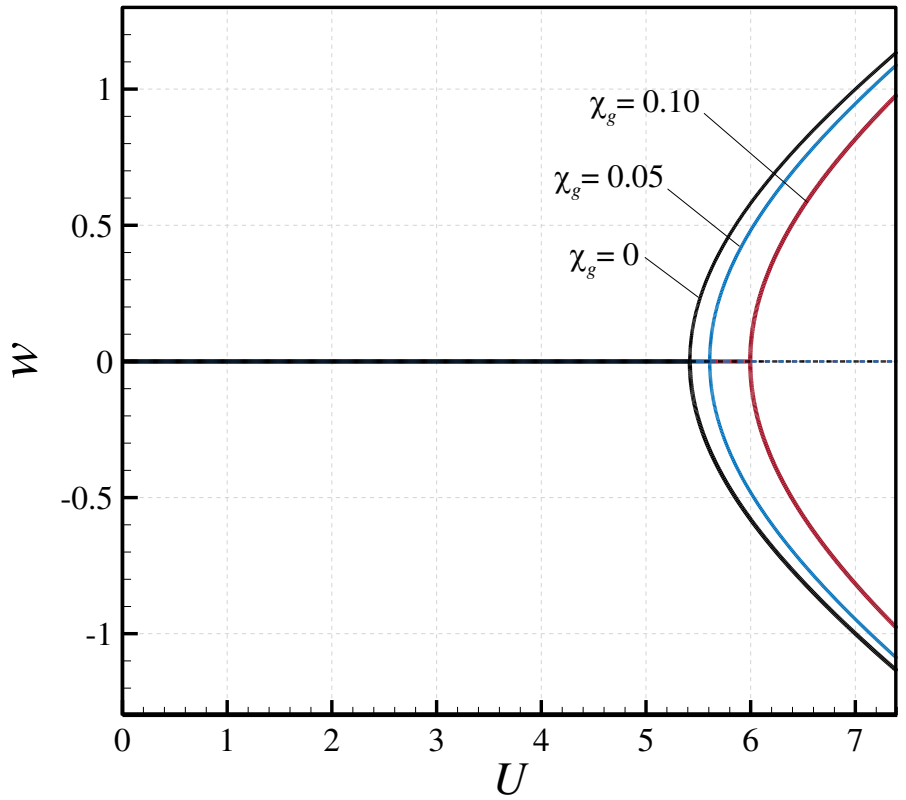

Figure 12: Small-scale effects on static bifurcation diagrams of the nanotube conveying nanofluid; (a) effect of χ_n when χ_g =0 (nonlocal theory); (b) effect of χ_g when χ_n =0 (strain gradient theory).

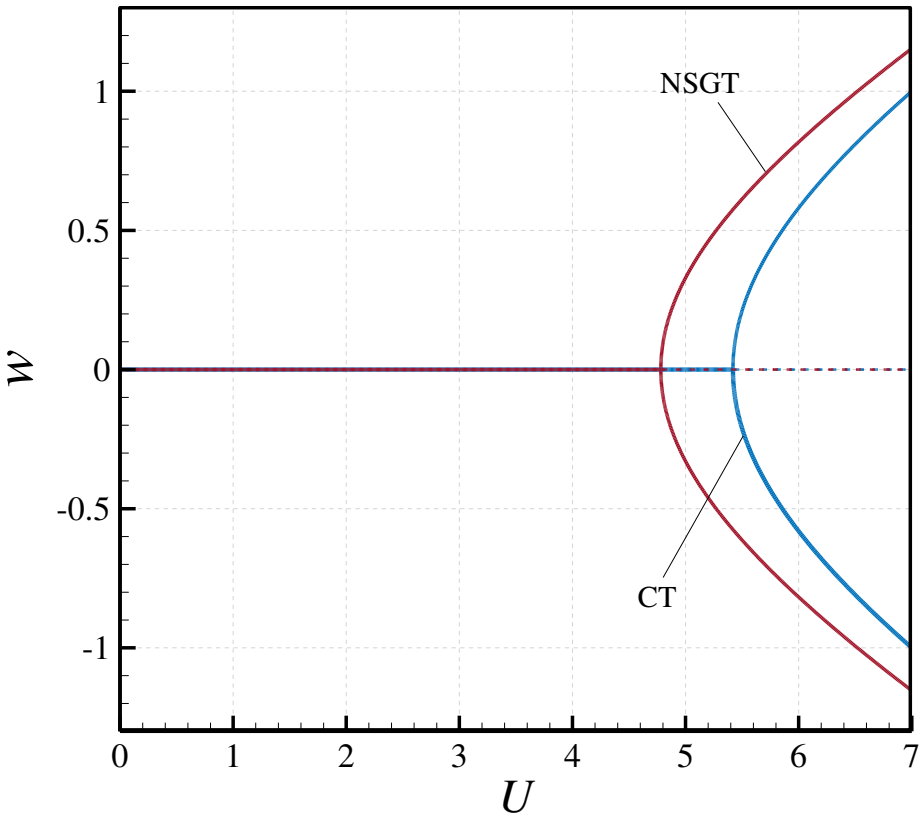

Figure 13: Comparison between the static bifurcation diagrams of the nanotube conveying nanofluid obtained via NSGT (with χ_n =0.09 and χ_g =0.03) and CT (equivalent to $\chi_n = \chi_g$ =0).